

## Article

# Experimentally Validated Coulomb Counting Method for Battery State-of-Charge Estimation under Variable Current Profiles

Bachir Zine <sup>1</sup>, Haithem Bia <sup>1</sup>, Amel Benmouna <sup>2,3,\*</sup>, Mohamed Becherif <sup>3,\*</sup> and Mehroze Iqbal <sup>3</sup> <sup>1</sup> Mechanical Engineering Department, Faculty of Technology, University of Eloued, El Oued 39000, Algeria<sup>2</sup> ESTA, School of Business and Engineering, 90000 Belfort, France<sup>3</sup> Femto-ST, FCLAB, University Bourgogne Franche-Comte, CNRS, UTBM, 91110 Belfort, France

\* Correspondence: amel.benmouna@utbm.fr (A.B.); mohamed.becherif@utbm.fr (M.B.)

**Abstract:** Battery state of charge as an effective operational indicator is expected to play a crucial role in the advancement of electric vehicles, improving the battery capacity and energy utilization, avoiding battery overcharging and over-discharging, extending the battery's useful lifespan, and extending the autonomy of electric vehicles. In context, this article presents a computationally efficient battery state-of-charge estimator based on the Coulomb counting technique with constant and variable discharging current profiles for an actual battery pack in real time. A dedicated experimental bench is developed for validation purposes, where pivotal measurements such as current, voltage, and temperature are initially measured during the charging/discharging cycle. The state of charge thus obtained via these measurements is then compared with the value estimated through the battery generic model. Detailed analysis with conclusive outcomes is finally presented to exhibit the flexible nature of the proposed method in terms of the precise state-of-charge estimation for a variety of batteries, ranging from lead–acid batteries for domestic applications to Li-ion batteries inside electric vehicles.

**Keywords:** state of charge; electric vehicle; coulomb counting approach; battery generic model



**Citation:** Zine, B.; Bia, H.; Benmouna, A.; Becherif, M.; Iqbal, M. Experimentally Validated Coulomb Counting Method for Battery State-of-Charge Estimation under Variable Current Profiles. *Energies* **2022**, *15*, 8172. <https://doi.org/10.3390/en15218172>

Academic Editor: Siamak Farhad

Received: 28 September 2022

Accepted: 25 October 2022

Published: 2 November 2022

**Publisher's Note:** MDPI stays neutral with regard to jurisdictional claims in published maps and institutional affiliations.



**Copyright:** © 2022 by the authors. Licensee MDPI, Basel, Switzerland. This article is an open access article distributed under the terms and conditions of the Creative Commons Attribution (CC BY) license (<https://creativecommons.org/licenses/by/4.0/>).

## 1. Introduction

The battery state of charge (SOC) for electric vehicles is equivalent to the oil meter for conventional fuel vehicles. Typically, the relation between the electrochemical reactions and SOC is complex and difficult to determine. In addition, for vehicles, the working conditions are challenging and complex. It is therefore very difficult to obtain precise SOC as it is a hidden state function of electrochemical reactions inside the battery. It is possible to separate the battery SOC estimation strategies into four classes [1]: characteristic param-driven approach [2–7], an integral estimation method [8–11], a physical model-driven method [12–16], and a data-driven approach [17–25], as illustrated in Figure 1.

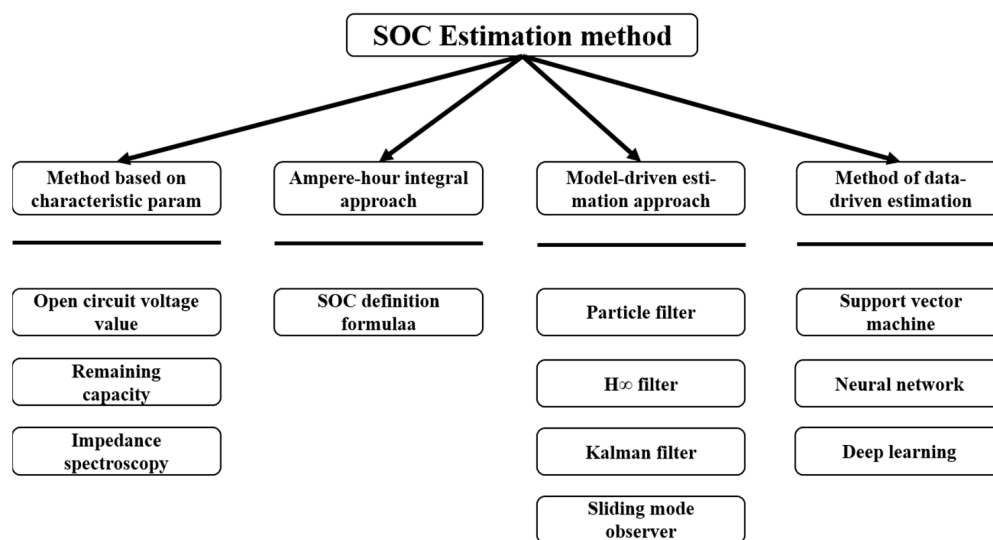


Figure 1. Classification of SOC estimation methods [26].

Subsequently, Table 1 sums up the benefits and drawbacks of four SOC assessment strategies, which are presented in Figure 1. Due to the importance of this topic, SOC estimation is rigorously investigated by several researchers. The work of [27] evaluated the SOC estimation via two model-based techniques that are the extended Kalman filter and the adaptive dual extended Kalman filter influenced by a fuzzy inference system. The experimental results demonstrate that the last technique provides a more precise indication of the battery SOC. The reference [28] is focused on optimizing the battery state of health within the domain of satellite applications. To enhance the performance of the system, the authors have taken into consideration different constraints linked to the battery SOC. For this, the Coulomb counting technique is used to estimate the battery SOC. Another study [29] treated the battery SOC as an operational indicator, which can influence the energy consumption of the electric vehicle [30]. Therefore, the SOC estimator is defined as the crude power consumption of the studied electrical vehicle (for more details, the reader can consult [31,32]).

The goal of this work is to estimate the SOC of a domestic-grade lead–acid battery through empirical measurements of battery voltage and current using the Ampere-hour integral estimation method with constant and variable C-rates for discharge current. There are many studies on the SOC estimation of lead–acid and Li-ion batteries, especially the Coulomb counting method [33,34]. However, the research work conducted in this article differentiates by investigating the discharging behavior of a lead–acid battery in extended and varying conditions.

Table 1. SOC estimation methods: benefits, drawbacks, accuracy, and robustness. Reprinted from Refs. [35,36].

Methodology	Benefits	Drawbacks	Precision	Sturdiness
Method based on characteristic param	<ul style="list-style-type: none"> <li>- simpler implementation</li> <li>- lower computing burden</li> <li>- Real-time application</li> </ul>	<ul style="list-style-type: none"> <li>- easily influenced by factors of uncertainty</li> <li>- standard OCV or information calibration is required</li> </ul>	poor	good

Table 1. Cont.

Methodology	Benefits	Drawbacks	Precision	Sturdiness
Ampere-hour integral approach	<ul style="list-style-type: none"> <li>- simpler implementation</li> <li>- lower computational burden</li> <li>- Real-time application</li> </ul>	<ul style="list-style-type: none"> <li>- exact initial value of SOC is required</li> <li>- use of a high precision sensor causes a cumulative error.</li> <li>- is affected by drift noise and ageing.</li> </ul>	average	poor
Model-driven estimation approach	<ul style="list-style-type: none"> <li>- high precision</li> <li>- closed loop regulation</li> <li>- Real-time application</li> <li>- Adaptive</li> </ul>	<ul style="list-style-type: none"> <li>- requires model precision</li> <li>- computational complexity</li> <li>- divergence of predicted outcomes</li> </ul>	excellent	excellent
Method of data-driven estimation	<ul style="list-style-type: none"> <li>- high precision</li> <li>- Suitable for nonlinear implementation</li> </ul>	<ul style="list-style-type: none"> <li>- computational complexity</li> <li>- offline training</li> </ul>	excellent	poor

For that, a dedicated test bench is prepared, and cross-validation is conducted under real-time scenarios and simulations. Finally, the performance of the proposed method is depicted by an evident comparison with the data provided by the manufacturer under variable operating conditions and with the generic battery model. It is worth mentioning here that the proposed method is generic and flexible in terms of its application, which is especially true for domestic-grade batteries as well as for modern Li-ion batteries present in electric vehicles. Moreover, the hysteresis effect is also taken into account considering the studied lead–acid battery.

The remainder of the paper is presented as: In Section 2, the battery management system is summarized by citing some references. The Coulomb counting method is highlighted in Section 3. In Section 4, the generic battery model is developed and comprehensively discussed. The experimental setup, which exhibits the feasibility and the applicability of the proposed approach for the lead–acid battery to attain adequate SOC values, is highlighted in Section 5. Section 6 is dedicated to the obtained results that are discussed in detail. Finally, the conclusions and the relevant perspectives are drawn in Section 7.

## 2. Battery Management System

The battery management system (BMS) is a technology that performs the micro-management of the battery pack in terms of its state of health (SOH). Figure 2 depicts a general layout of a typical BMS, which constitutes numerous sensors, actuators, controllers, connection lines, etc. The bidirectional communication between the control unit of BMS and external bodies such as the human media interface is typically carried out via CAN (the communication bus controller area network). Besides maintaining reliability during normal and abnormal operating conditions, adequate provision of the battery state of charge to the vehicle's vehicle control unit (VCU) is among the vital tasks of BMS.

A well-built BMS aids in collecting critical data in real time, such as electrical measurements, temperature, and other relevant data via inherent sampling hardware. The collected data is then exploited via embedded algorithms and strategies to estimate the battery states, such as SOC [37], SOH [38], SOP [39], and RUL [40]. These states are ultimately fed to VCU, in order to facilitate effective power management.

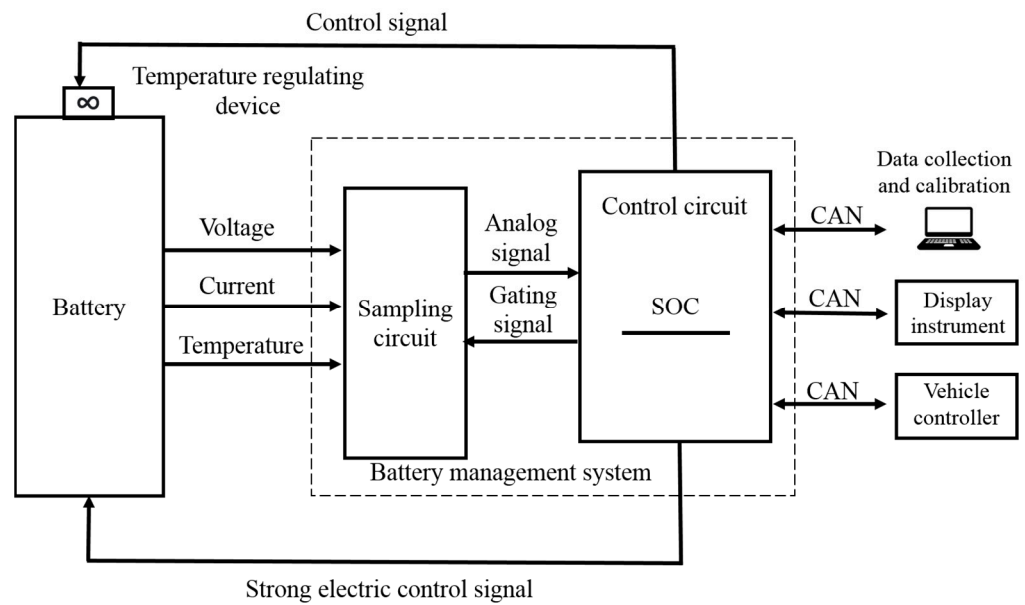


Figure 2. Schematic diagram of a typical BMS [26].

### 3. Coulomb Counting Method

The Coulomb counting method (known as the current integration method) is chosen as the baseline in this article and is among the most exploited method [41]. It consists of measuring the battery open circuit voltage at the start-up to estimate the initial SOC using the battery datasheet information. Then, the battery current information is integrated to estimate the amount of charge delivered (or recovered) by the batteries. The overall concept is presented in Equation (1), where knowledge of the initial SOC is detrimental to determining the state of charge [24,42,43]. Based on this approach, the SOC for the battery pack is calculated as follows [44]:

$$\text{SOC} = \text{SOC}_0 - \frac{1}{C_N} \int_{t_0}^t \eta \cdot I(\tau) d\tau \quad (1)$$

If the initial value of the charge state  $\text{SOC}_0$  is specified, or imposed (technically, most researchers impose the initial state as to be fully charged or fully discharged), the Coulomb counter provides precise estimation with relative ease and simplicity [45]. On the contrary, this method is less accurate if the  $\text{SOC}_0$  is unknown.

The Coulomb counting strategy computes the remaining stored energy essentially by collecting the charge moved in or out of the battery. The precision of this strategy depends fundamentally on a real estimation of the battery current and a precise assessment of the initial SOC. With pre-knowledge of the initial SOC, which also can be stored at the end of the vehicle trip in a flash memory to be reused as the initial SOC for the next trip (and neglecting the battery self-discharge), the battery SOC can be determined by computing the stored and the released energy flows over the operating time. Nevertheless, the stored energy in the battery is not completely available to be used due to the DOD (depth of discharge) which is a quantity of energy to keep inside the battery to avoid permanent damage. Moreover, there are losses during the charging and discharging process. For an exact SOC assessment, this effect should be considered [46]. Furthermore, the SOC must be recalibrated consistently, and the discharge limit should be considered for an exact assessment.

### 4. Generic Battery Model

The battery model can be obtained by considering a voltage source in series with constant resistance, as appears in Equation (2) [11].

$$V_{batt} = E_0 - K \frac{Q}{Q - i_t} \cdot i_t - R \cdot I + A \cdot \exp(-B \cdot i_t) K \frac{Q}{Q - i_t} \cdot i^* \tag{2}$$

As depicted in Figure 3, the special feature of this model is the use of filtered current ( $i^*$ ) through the polarization resistance. This filtered current solves the problem of the algebraic loop due to the simulation of power systems in Simulink [47]. Despite the existence of hysteresis between the charging and discharging of the battery voltage, this model is still valid for both charge and discharge cycles [48]. The battery models can be obtained using:

- ✓ The charge model ( $i^* < 0$ )

$$f_1(i_t, i^*, exp, batt\ type) = E_0 - K \frac{Q}{i_t - 0.1Q} \cdot i^* - K \frac{Q}{i_t - Q} \cdot i_t + \text{Exp}(t) \tag{3}$$

- ✓ The discharge model ( $i^* > 0$ )

$$f_1(i_t, i^*, exp, batt\ type) = E_0 - K \frac{Q}{i_t - Q} \cdot i^* - K \frac{Q}{i_t - Q} \cdot i_t + \text{Exp}(t) \tag{4}$$

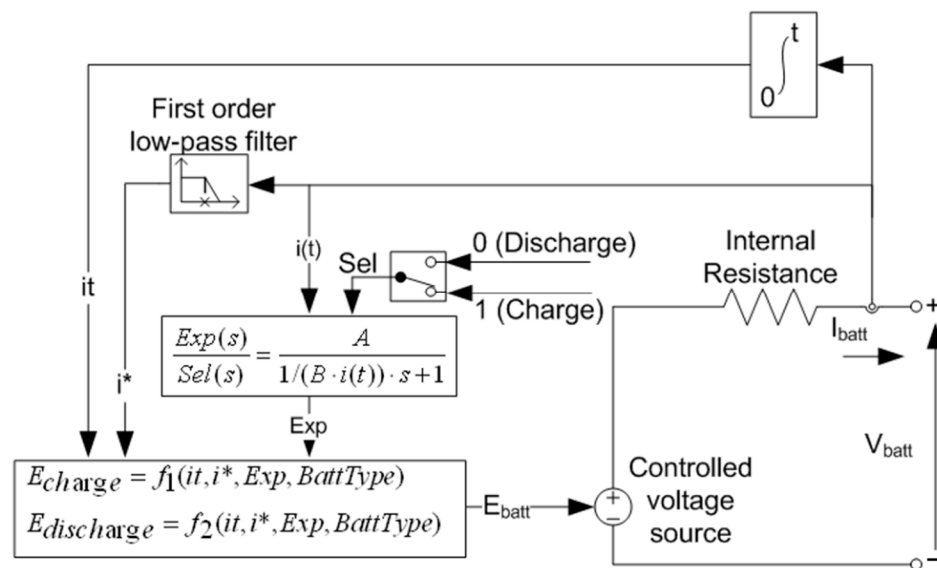
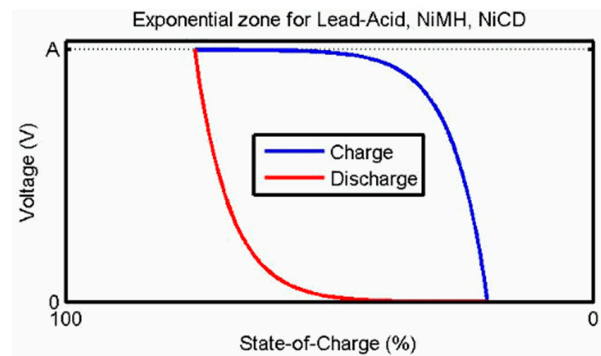


Figure 3. Graphical description of the employed battery model.

The employed model is simplistic and cannot exactly mimic the complex electrochemical reactions taking place within the battery under the influence of actual operating conditions. However, this model is still adequate from the computational side, and can suffice for a range of applications. Especially, for the discharge state of lead acid batteries with different currents, which is extensively studied, where the discharge curve of the simulations matches with the discharge curve of the experimental work and with that of the datasheet. Therefore, even with assumptions and limitations, the utilized model suffices the fundamental needs of this research work. It is worth mentioning here that the hysteresis phenomenon for the lead–acid battery is considered here. The effect can be seen in Figure 4, exhibiting that the exponential voltage increases when the battery is charging, while during the discharging, the exponential voltage decreases immediately.



**Figure 4.** Hysteresis effect associated with the lead–acid battery.

**Application:** From the discharge curve provided by the manufacturer, the extracted parameters are presented in Table 2. The model also has its assumptions and limitations as follows:

✓ **Limitations**

- The minimum no-load battery voltage is 0 V and the maximum battery voltage is equal to  $2 \times E_0$ .
- The minimum capacity of the battery is 0 Ah and the maximum capacity is  $Q_{max}$ .

✓ **Assumptions**

- The internal resistance is supposed as a constant value during the charge and the discharge cycles and does not vary with the amplitude of the current.
- The parameters of the model are deduced from discharge characteristics and assumed to be the same for charging.
- The capacity of the battery does not change with the amplitude of the current (no Peukert effect).
- The model does not take the temperature into account.
- The self-discharge of the battery is not represented. It can be represented by adding a large resistance in parallel with the battery terminals.
- The battery has no memory effect.

**Table 2.** Battery parameters: discharge at variable C-rate.

C-Rates of Discharge	0.25 C	0.17 C	0.09 C	Different C-Rates
Nominal voltage (V)	12	12	12	12
Rated capacity (Ah)	52	52	52	52
Initial state-of-charge (%)	100	100	100	100
Max. capacity (Ah)	40.1999	53.8	47.5	47.5
Fully charged voltage (V)	12.7	12.8	12.9	12.9
Nominal discharge current (A)	13	8.84	4.68	12
Internal resistance ( $\Omega$ )	0.0055	0.0055	0.0055	0.0055
Capacity (Ah) @ nominal voltage	38.2	44.80	46	46
Exp. zone [Voltage(V), capacity(Ah)]	[12.7, 2.5]	[12.8, 1.9]	[12.9, 2.225]	[12.9, 2.225]

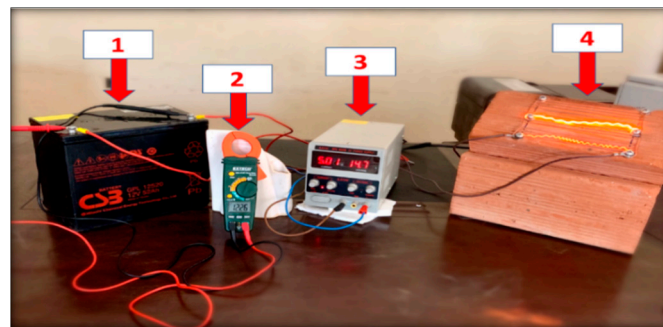
## 5. Experimental Method and Description

**Battery specification:** The battery employed in this research is a valve-regulated lead–acid (VRLA) type with a nominal voltage of 12 V and a nominal capacity of 52 Ah. The recommended voltage when charged for standby use is 1.75 V for a single cell (6 cells in series). Further features of this battery are presented in Table 3.

**Table 3.** Lead–acid battery parameters.

Cells per unit	6
Voltage per unit	12 V
Capacity	52 Ah @ 20 h-rate to 1.75 V per cell @25 °C (77 °F)
Weight	Approx. 18 Kg (39.68 lbs.)
Maximum discharge current	500 A (5 s)
Internal resistance	Approx. 5.5 mΩ
Operating temperature range	Discharge: −15 °C~50 °C (5 °F~122 °F) Charge: −15 °C~40 °C (5 °F~104 °F) Storage: −15 °C~40 °C (5 °F~104 °F)
Float charging voltage	13.5 to 13.8 VDC/unit Average at 25 °C (77 °F)
Maximum charging current limit	15.6 A
Equalization and cycle service	14.4 to 15.0 VDC/unit Average at 25 °C (77 °F)
Self discharge	Batteries can be stored for 6 months at 25 °C (77 °F).

**Measurement test bench:** The measurement test bench is presented in Figure 5, which further consists of four interconnected components.

**Figure 5.** The test bench.

1. Lead–acid battery
2. Clamp meter
3. DC power supply
4. Variable resistor (handmade)

**Computing parameters:** The proposed computing method is implemented in Matlab/Simulink version 2015b and has the following attributes and parameters: variable step, ode45 (Dormand–Prince), relative tolerance =  $1 \times 10^{-3}$ , time tolerance =  $10 \times 128 \times \text{eps}$ , zero crossing control = use local settings, algorithm = non adaptive, number of consecutive zero crossings = 1000, number of consecutive min steps = 1.

**Charging process test:** The battery is charged via an external DC power supply, and the initial voltage at the time of testing is effectively set at 14.7 V. The current maximum limit is set to 5.03 A (this is the maximum available value). The battery is connected to the power supply and is left until its fully charged. The voltage and current are measured using a voltmeter and clamp meter every 10 min. The end-of-charge voltage equals  $V_{\text{finish-ocv}} = 13.96$  V and the end-of-charge current (the minimum value of the current in the vicinity of full charge) is  $I_{\text{min}} = 0.29$  A. When the charging current reaches the minimum value of 0.29 A (indicated by the manufacturer), the battery is disconnected, and the DC power voltage supply is turned off. This test was spanned over 02 days, the duration of this test, therefore, equals  $T_{\text{ch}} = 1440$  min or  $T_{\text{ch}} = 24$  h.

**Discharging process test:** Two experiments are conducted in total with relevance to the discharging test:

- *Discharging with constant C-rates:* a variable resistor is connected (for adjustment to variable C-rates, that is to reach discharge current at 0.25 C, 0.17 C, and 0.09 C respectively) with the battery. Consequently, the voltage and the discharge current are measured after every 5 min by using a clamp meter. After 3.05, 5.41, and 10.25 h, respectively (corresponding to the associated C-rate), it reaches the lower permissible limit of discharge voltage (cut-off voltage) 10.10, 10.37, and 10.39 V each. Afterwards, the discharge resistance is disconnected. The discharge resistance equaled  $R_{\text{disch}} = [0.96\text{--}1] \Omega$ ,  $[1.42\text{--}1.50] \Omega$ , and  $[2.69\text{--}3] \Omega$ , with the ambient temperature  $T = 26.7^\circ$ ,  $28.6^\circ$ , and  $26.1^\circ \text{C}$ .
- *Discharging with variable C-rates:* the variable resistor is connected (for adjustment to variable C-rates discharge current 0.23 C, 0.115 C, and 0.057 C, respectively). These values of C-rates correspond to having three resistances connected in parallel. The value of each resistance is  $3.225 \Omega$ . During the first period, the discharge is performed at 0.23 C until 1.11 h. After that, the first resistance is disconnected, then the discharge continues at 0.115 C until 4.44 h. At this point, the second resistance is also disconnected. The discharge is pursued then with 0.057 C until 7.23 h, and at this moment, even the last resistance is disconnected, and the experiment is stopped. The battery voltage and discharging current are measured every 5 min with a clamp meter during the whole experimental session. After 7.23 h, the end of discharge is reached (cut-off voltage) which is equal to 10.39 V. At this point, the discharge resistance is completely disconnected. It is also worth mentioning that the ambient temperature equaled  $T = 27.1^\circ \text{C}$  (approx.) during the experimental session.

## 6. Results and Discussion

As depicted in Figure 6: the discharge voltage at 0.25 C, 0.17 C, and 0.09 C decreases to 10.10 V, 10.37 V, and 10.39 V, respectively, during 3.05, 5.41, and 10.25 h. These values are called the cut-off voltages, i.e., when the battery discharge voltage has reached the lowest permissible value. At this point, the battery is disconnected to avoid permanent damage. The 10.10 V, 10.37 V, and 10.39 V values are not indicative of the total discharge (SOC = 0%) but correspond to the minimum SOC value in the vicinity of 20%, also known as depth of discharge (DoD) [49].

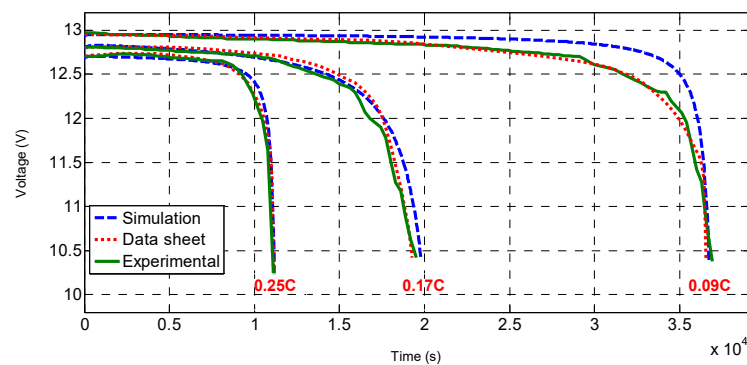


**Figure 6.** The discharge voltage vs. time at 0.25/0.17 and 0.09 C.

It can be observed that the experimental discharge curve is very close to the simulated one, except for the sensor's noise and deviation in the collected points. This difference shows that battery power varies according to the operating conditions and user parameters (charging mode, ambient temperature, discharge current, etc.). It should be noted that the manufacturer-provided data normally correspond to ideal conditions ( $T = 25^\circ \text{C}$ ,  $I_{\text{disch}} = 13 \text{ A}$ ,  $8.84 \text{ A}$ , and  $4.68 \text{ A}$ , respectively) and the battery's aging status (SOH = 100%), which means a new battery. So, during the experiments, it is found that the 03 sets (datasheet, simulated, and experimental) are close, this indicates that the battery model used shows a very high precision in the discharge phase of the battery.

Figure 7 depicts the results corresponding to estimated SOC evolution with discharging at fixed C rates. It can be observed that the battery is initially fully charged ( $SOC_0 = 100\%$ ) and that the battery charging status decreases to a minimum value ( $SOC_{min} = 20\%$ ) after 3.05, 5.41, and 10.25 h, respectively. This value must not exceed to prevent the battery from being permanently damaged, as depicted in [50] for the application of hybrid electric vehicles. The straight line is the SOC curve calculated by the Coulomb counting estimator, i.e., the battery is discharged at a constant discharge current ( $I_{disch} = 13$  A, 8.84 A, and 4.68 A, respectively). This approach facilitates the battery's SOC evolution over the entire discharge cycle (3.05 h, 5.41 h, and 10.25 h, respectively).

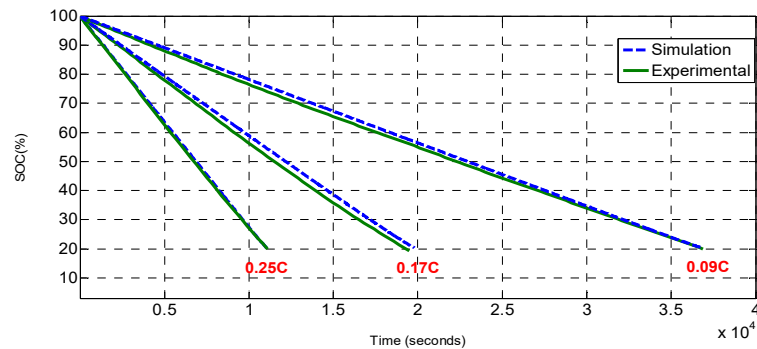


Figure 7. The SOC as a function of time at fixed C rates.

All the tests evidently reflect that the experimental SOC and the simulated ones are very close. This shows that this technique is very accurate and useful thanks to its simplicity of implementation and calculations. Additionally, it is easy to implement, since it only exploits the data received from current and voltage sensors.

Figure 8 exhibits the result of battery discharge at variable C rates using a handmade variable resistor (three equal resistors connected in parallel), where the total equivalent resistor equals  $R_{eq1} = 1.075$  ohms. At the beginning, all resistors are connected and a discharging rate of 0.23 C is applied from [0 to 1.11 h]. Then, one resistance is disconnected from the total equivalent resistors to obtain  $R_{eq2} = 2.15$  ohms, corresponding to a discharge rate of 0.115 C from [1.11 to 4.44 h]. Finally, a second resistance is disconnected, which means that only one resistance is kept connected, with a value of 3.225 ohms, corresponding to a discharging rate of 0.057 C from [4.44 to 7.23 h].

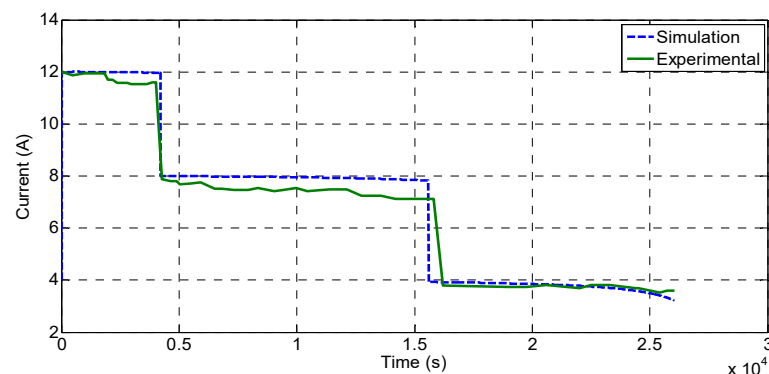
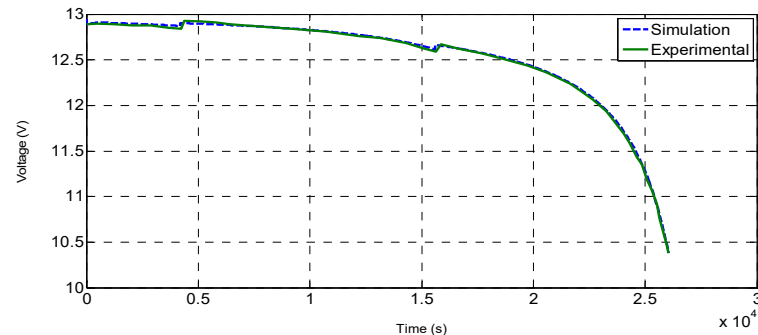


Figure 8. The discharge current as a function of time at variable C-rates.

Therefore, it is noticed that the current is constant during each C-rates of the discharging range. This is a safe and effective method. Where the minimum value of discharging current is 2.90 A, which corresponds to a cutting voltage of 10.39 V.

Figure 9 illustrates that with the applied variable C-rates, the discharge voltage decreases to 10.39 V over the period of 7.23 h. From the presented curve, it can be noticed that the three ranges express the discharging process with the different C-rates: 0.23 C,

0.115 C, and 0.057 C, respectively. The two curves (simulated and experimental) are almost identical, exhibiting that the generic battery presents the real behavior of the battery pack during the discharging process with very high precision.



**Figure 9.** The discharge voltage as a function of time at variable C-rates.

The evolution of estimated SOC under the influence of variable C rates is depicted in Figure 10. It can be observed that the battery is initially fully charged (SOC<sub>0</sub> = 100%) and the battery charging status decreases after 7.23 h to its minimum threshold (SOC = 20%), corresponding to the recommended value of the lead–acid battery (SOC<sub>min</sub> = 20%). Again, this value must not exceed to prevent the battery from being permanently damaged. Furthermore, the theoretical estimation matches the experimental findings.

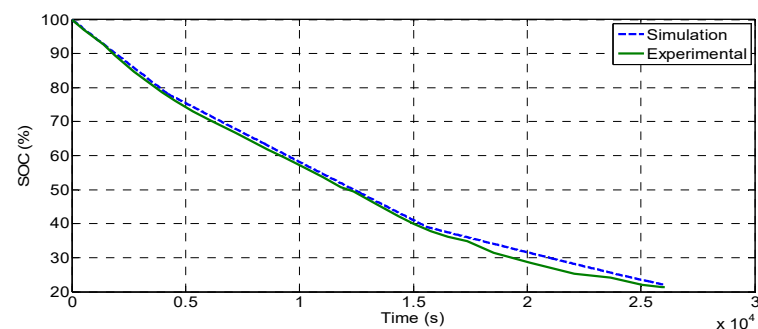


**Figure 10.** The SOC as a function of time at variable C rates.

The SOC curve calculated by the Coulomb counting estimator is nearly a straight line (in their specific regions), i.e., the discharging test is performed individually under variable discharge currents for sustained periods ( $I_{\text{disch}} = 12 \text{ A}$ ,  $6 \text{ A}$  then  $3 \text{ A}$ , respectively). It can be observed that the SOC<sub>experimental</sub> and SOC<sub>simulated</sub> are almost the same, which shows that this technique is accurate and useful.

Finally, Figure 11 exhibits the two curves (datasheets and simulation), depicting that the initial value of the battery charge current is equal to 5.5 A and 5.03 A. It can be noticed that the charging current stays constant for 3.50 h at a value of 5.5 A in datasheet/simulations, while 5.03 A in the experimental curve. Then the value decreases until 0.29 A in all the cases whether experimental or simulations. One can distinguish two areas on the curve where the first is from [0 to 3.20] h in the experimental curve and from [0 to 3.50] h in the simulation and datasheet curves. These curves are the representation of the charging process via constant current (CC) and by a constant voltage (CV). The only difference between the three curves (datasheet, simulation, and experimental) is in the zone of charge by a constant current and exactly in the initial value given, wherein the experimental test, it is set to a value of 5.03 A only (which is the maximum available power supply value). In contrast, the value of the datasheet and simulation is 5.5 A.

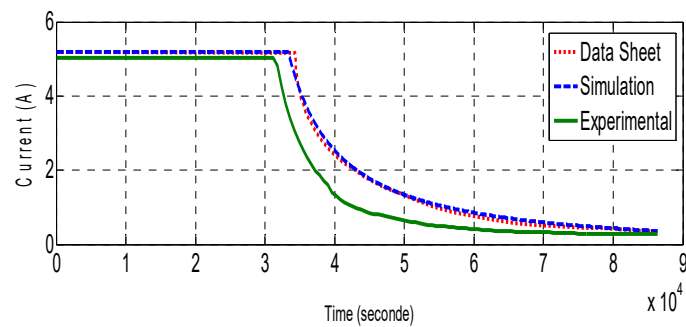


**Figure 11.** The charging current as the function of time.

Figure 12 indicates the fact that the battery voltage at the start of this test is set to 11.6 V in the three curves (experimental, datasheets, and simulations). Moreover, the initial charge condition is  $SOC_0 = 20\%$  [44]. It can be observed that the charge voltage rises rapidly up to 14.7 V and stabilizes at this value, i.e., two curve areas are distinguished where the first is from [0 to 3] h in the experimental/datasheet curve, and from [0 to 2.5] h in the simulated curve, intended for the constant current (CC) charging mode [45]. The second distinguishable area is from [3 to 20] h intended for the charging mode using a constant voltage (CV) mode.

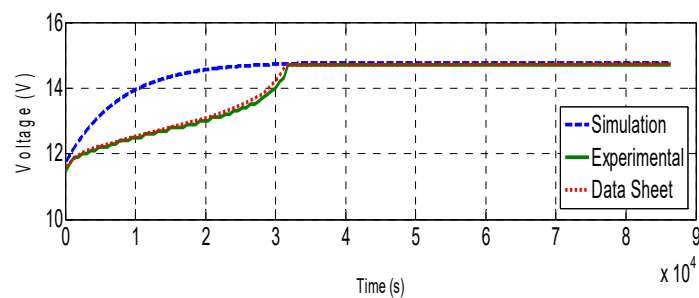


**Figure 12.** Charging voltage as the function of time.

The only difference between the three curves (experimental, datasheet, and simulated) is in the zone of charge by a constant current (the duration of this phase is different as in the datasheet/experimental is 3 h and in simulations is 2.5 h). This is because the simulation parameters in the discharge phase are the same as for the charging phase. After all, the charging phase is dependent on numerous factors such as charging mode, initial SoC, ambient temperature, and mode of charging. This leads to a charge period of 24 h when the end-of-charge current is equal to 0.29 A to prevent overcharging the battery by turning off the DC power supply.

In Figure 13, the  $SOC_0$  equals 20% at time  $t = 0$  and increases with the relation of charging up to 100%, i.e., the battery is fully charged.

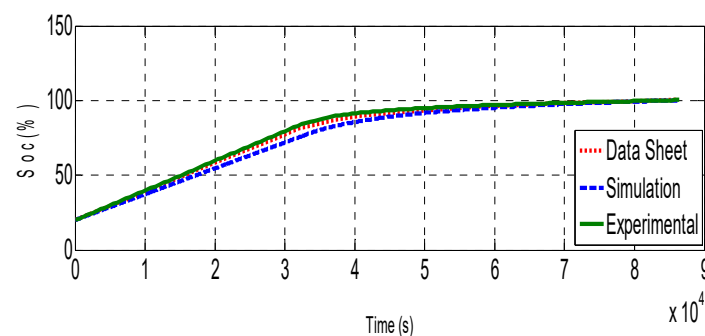


**Figure 13.** The SOC as function of time.

There are two parts in the curve, from [0 to 3.5] h is the first portion, which corresponds to the constant current charging mode. It has almost a linear shape. This part is characterized by the rapid variation of the SOC as a time-dependent variable for instance at 3.5 h SOC (experimental) = 85%, SOC (datasheet) = 83% and SOC (simulation) = 80%. The second part is in the form of a nonlinear curve line. It corresponds to the charging mode at a constant voltage; it is characterized by the slow variation of the SOC. For example, during [3.5–24] h, the SOC (experimental) increases by 15%, SOC (datasheet) increases by 17%, and SOC (simulation) increased by 20%.

Hence, it can be said that the battery charge capacity is dependent on the charging mode, it is faster in CC mode and slower in CV mode, which is why the new charger is faster to gain more time, especially in the lead–acid batteries.

From Figure 13, the Coulomb counter approach provides a fair depiction of SOC during the entire charge; as a result, one can say that this method is independent of the battery's model and technology.

## 7. Conclusions and Perspectives

This study presents a Coulomb counting technique-based battery state-of-charge estimator with constant and variable discharging current profiles for a real battery pack in a real-time environment. The following conclusions are drawn from this study:

In the charging mode, the battery model used in the MATLAB Simulink is less efficient. Regardless, it is widely used and has excellent battery economy when discharged at a constant current. That is the reason why it is also included for the sake of comparison.

The only short-coming of the Coulomb counting method is the difficulty of estimating the initial SOC. High-precision estimation sensors (for voltage and current) are also needed, so these instruments need to be periodically modified.

Lead–acid batteries are only suitable for short-range vehicles. They remain the cheapest form of battery and are likely to be used for these purposes. A lot of useful and small-scale EVs that do not require a long-range can be made via lead–acid batteries.

Most commercial-scale EVs require an extended traveling range; therefore, modern Li-ion batteries can serve the purpose. The proposed SOC estimator is expected to provide quick and reliable information, which can be then integrated into energy management.

It is concluded that constant current discharge is quicker, which is the approach used for fast charging, and it is shown in this work that the efficiency of the generic battery model is competitive, as its findings are close to experimental work. The Coulomb counter approach is useful for estimating the battery SOC; also, in this case, the discharge with variable discharge currents is always correct.

By using simple calculations and hardware requirements, the proposed method can therefore be systematically implemented in any portable devices as well as electric cars. In this research, the ampere-hour integral method is validated experimentally via a domestic lead–acid battery. It is worth mentioning here that the proposed method is generic in its implementation. Given that, the implementation and application of modern Li-ion batteries are reserved for future studies.

**Author Contributions:** Conceptualization, results analysis, managerial insights, and methodology are performed by B.Z.; H.B. was involved in writing original draft preparation. Formal analysis and investigations were performed by A.B.; M.B. was involved in writing the reviews and managing the references. Finally, M.I. performed language correction and general organization. All authors have read and agreed to the published version of the manuscript.

**Funding:** This work was not funded by any organization and/or society in any capacity.

**Conflicts of Interest:** The authors have no conflict of interest to declare that are relevant to the content of this article.

## Abbreviations

SOC	State of charge
Ah	Ampere hour
OCV	Open circuit voltage
AC	Alternative current
SOH	State of health
CC	Constant current
CV	Constant voltage
$C_N$	Nominal capacity of the battery
$\eta$	Coulomb efficiency
$I(\tau)$	The current versus time (negative during charge and positive during discharge)
$V_{batt}$	The battery voltage (V)
$E_0$	The constant battery voltage (V)
K	The polarization constant (V/(Ah)) or polarization resistance ( $\Omega$ )
Q	The battery capacity (Ah)
$i_t$	$= \int Idt$ : actual battery charge (Ah)
A	The exponential voltage (V)
B	The exponential capacity (Ah) – 1
R	The internal resistance ( $\Omega$ )
I	The battery current (A)
$i^*$	The filtered current (A)
$I_{dis}$	The value of the current of discharge
SOC <sub>0</sub>	Initial state of charge
SOC <sub>min</sub>	Minimum state of charge
SOC <sub>exp</sub>	Experimental state of charge
SOC <sub>th</sub>	Theoretical state of charge
V <sub>ch<sub>int</sub></sub>	Initial charge voltage
V <sub>ch<sub>end</sub></sub>	End charge voltage
T <sub>ch<sub>sum</sub></sub>	Simulation charge time
V <sub>dis<sub>int</sub></sub>	Initial discharge voltage
V <sub>dis<sub>end</sub></sub>	End discharge voltage
T <sub>dis<sub>sum</sub></sub>	Simulation discharge time
VRLA	Valve regulated lead–acid battery
BMS	Battery management system
VCU	Vehicle control unit
SOP	State of power
RUL	Remaining useful life
DOD	Depth of discharge

## References

1. Yang, R.; Xiong, R.; He, H.; Chen, Z. A fractional-order model-based battery external short circuit fault diagnosis approach for all-climate electric vehicles application. *J. Clean. Prod.* **2018**, *187*, 950–959. [[CrossRef](#)]
2. Rodrigues, S.; Munichandraiah, N.; Shukla, A. A review of state-of-charge indication of batteries by means of a.c. impedance measurements. *J. Power Sources* **2000**, *87*, 12–20. [[CrossRef](#)]
3. Huet, F. A review of impedance measurements for determination of the state-of-charge or state-of-health of secondary batteries. *J. Power Sources* **1998**, *70*, 59–69. [[CrossRef](#)]
4. Weng, C.; Sun, J.; Peng, H. A unified open-circuit-voltage model of lithium-ion batteries for state-of-charge estimation and state-of-health monitoring. *J. Power Sources* **2014**, *258*, 228–237. [[CrossRef](#)]
5. Dubarry, M.; Svoboda, V.; Hwu, R.; Liaw, B.Y. Capacity loss in rechargeable lithium cells during cycle life testing: The importance of determining state-of-charge. *J. Power Sources* **2007**, *174*, 1121–1125. [[CrossRef](#)]
6. Schmidt, J.P.; Chrobak, T.; Ender, M.; Illig, J.; Klotz, D.; Ivers-Tiffée, E. Studies on LiFePO<sub>4</sub> as cathode material using impedance spectroscopy. *J. Power Sources* **2011**, *196*, 5349–5355. [[CrossRef](#)]
7. He, H.; Xiong, R.; Guo, H. Online estimation of model parameters and state-of-charge of LiFePO<sub>4</sub> batteries in electric vehicles. *Appl. Energy* **2012**, *89*, 413–420. [[CrossRef](#)]
8. Zhang, Y.; Song, W.; Lin, S.; Feng, Z. A novel model of the initial state of charge estimation for LiFePO<sub>4</sub> batteries. *J. Power Sources* **2014**, *248*, 1028–1033. [[CrossRef](#)]

9. Wang, J.; Cao, B.; Chen, Q.; Wang, F. Combined state of charge estimator for electric vehicle battery pack. *Control Eng. Pract.* **2007**, *15*, 1569–1576. [[CrossRef](#)]
10. Becherif, M.; Pera, M.; Hissel, D.; Jemei, S. Estimation of the lead-acid battery initial state of charge with experimental validation. In Proceedings of the 2012 IEEE Vehicle Power and Propulsion Conference, Seoul, Korea, 9–12 October 2012; pp. 469–473.
11. Ng, K.S.; Moo, C.-S.; Chen, Y.-P.; Hsieh, Y.-C. Enhanced coulomb counting method for estimating state-of-charge and state-of-health of lithium-ion batteries. *Appl. Energy* **2009**, *86*, 1506–1511. [[CrossRef](#)]
12. Chan, C.; Lo, E.; Weixiang, S. The available capacity computation model based on artificial neural network for lead–acid batteries in electric vehicles. *J. Power Sources* **2000**, *87*, 201–204. [[CrossRef](#)]
13. Gu, W.B.; Wang, C.Y. Thermal-Electrochemical Modeling of Battery Systems. *J. Electrochem. Soc.* **2000**, *147*, 2910–2922. [[CrossRef](#)]
14. Zhang, Y.; Xiong, R.; He, H.; Shen, W. Lithium-Ion Battery Pack State of Charge and State of Energy Estimation Algorithms Using a Hardware-in-the-Loop Validation. *IEEE Trans. Power Electron.* **2016**, *32*, 4421–4431. [[CrossRef](#)]
15. Xiong, R.; He, H.; Sun, F.; Zhao, K. Evaluation on State of Charge Estimation of Batteries With Adaptive Extended Kalman Filter by Experiment Approach. *IEEE Trans. Veh. Technol.* **2012**, *62*, 108–117. [[CrossRef](#)]
16. Plett, G.L. Extended Kalman filtering for battery management systems of LiPB-based HEV battery packs Part 2. Modeling and identification. *J. Power Sources* **2004**, *134*, 262–276. [[CrossRef](#)]
17. Cuadras, A.; Kanoun, O. Soc li-ion battery monitoring with impedance spectroscopy. In Proceedings of the 2009 6th International Multi-Conference on Systems, Signals and Devices, SSD, Djerba, Taiwan, 23–26 March 2009.
18. Chau, K.; Wu, K.; Chan, C. A new battery capacity indicator for lithium-ion battery powered electric vehicles using adaptive neuro-fuzzy inference system. *Energy Convers. Manag.* **2004**, *45*, 1681–1692. [[CrossRef](#)]
19. Wang, Z.; Xu, J.; Wang, T. The online monitoring system software design and the SOC estimation algorithm research for power battery. In Proceedings of the 2013 IEEE International Conference on Vehicular Electronics and Safety, ICVES 2013, Dongguan, China, 28–30 July 2013; pp. 89–92.
20. Lv, J.; Yuan, H.; Lv, Y. Battery state-of-charge estimation based on fuzzy neural network and improved particle swarm optimization algorithm. In Proceedings of the 2012 2nd International Conference on Instrumentation and Measurement, Computer, Communication and Control, Washington, DC, USA, 8–10 December 2012; pp. 22–27.
21. Chemali, E.; Kollmeyer, P.J.; Preindl, M.; Ahmed, R.; Emadi, A.; Kollmeyer, P. Long Short-Term Memory Networks for Accurate State-of-Charge Estimation of Li-ion Batteries. *IEEE Trans. Ind. Electron.* **2018**, *65*, 6730–6739. [[CrossRef](#)]
22. He, W.; Williard, N.; Chen, C.; Pecht, M. State of charge estimation for Li-ion batteries using neural network modeling and unscented Kalman filter-based error cancellation. *Int. J. Electr. Power Energy Syst.* **2014**, *62*, 783–791. [[CrossRef](#)]
23. Kang, L.; Zhao, X.; Ma, J. A new neural network model for the state-of-charge estimation in the battery degradation process. *Appl. Energy* **2014**, *121*, 20–27. [[CrossRef](#)]
24. Junping, W.; Quanshi, C.; Binggang, C. Support vector machine based battery model for electric vehicles. *Energy Convers. Manag.* **2006**, *47*, 858–864. [[CrossRef](#)]
25. Li, I.-H.; Wang, W.-Y.; Su, S.-F.; Lee, Y.-S. A Merged Fuzzy Neural Network and Its Applications in Battery State-of-Charge Estimation. *IEEE Trans. Energy Convers.* **2007**, *22*, 697–708. [[CrossRef](#)]
26. Xiong, R.; Shen, W. *Advanced Battery Management Technologies for Electric Vehicles*; John Wiley & Sons: Hoboken, NJ, USA, 2019; pp. 1–297.
27. Yang, K.; Chen, Z.; He, Z.; Wang, Y.; Zhou, Z. Online estimation of state of health for the airborne Li-ion battery using adaptive DEKF-based fuzzy inference system. *Soft Comput.* **2020**, *24*, 18661–18670. [[CrossRef](#)]
28. Lami, M.; Shamayleh, A.; Mukhopadhyay, S. Minimizing the state of health degradation of Li-ion batteries onboard low earth orbit satellites. *Soft Comput.* **2019**, *24*, 4131–4147. [[CrossRef](#)]
29. Modi, S.; Bhattacharya, J.; Basak, P. Convolutional neural network–bagged decision tree: A hybrid approach to reduce electric vehicle’s driver’s range anxiety by estimating energy consumption in real-time. *Soft Comput.* **2020**, *25*, 2399–2416. [[CrossRef](#)]
30. Iqbal, M.; Becherif, M.; Ramadan, H.S.; Badji, A. Dual-layer approach for systematic sizing and online energy management of fuel cell hybrid vehicles. *Appl. Energy* **2021**, *300*, 117345. [[CrossRef](#)]
31. Kularatna, N. *Dynamics, Models, and Management of Rechargeable Batteries*; Academic Press: Cambridge, MA, USA, 2015.
32. Iqbal, M.; Laurent, J.; Benmouna, A.; Becherif, M.; Ramadan, H.S.; Claude, F. Ageing-aware load following control for composite-cost optimal energy management of fuel cell hybrid electric vehicle. *Energy* **2022**, *254*, 124233. [[CrossRef](#)]
33. Salazar, D.; Garcia, M. Estimation and Comparison of SOC in Batteries Used in Electromobility Using the Thevenin Model and Coulomb Ampere Counting. *Energies* **2022**, *15*, 7204. [[CrossRef](#)]
34. González, I.; Ramiro, A.; Calderón, M.; Calderón, A.; González, J. Estimation of the state-of-charge of gel lead-acid batteries and application to the control of a stand-alone wind-solar test-bed with hydrogen support. *Int. J. Hydrogen Energy* **2012**, *37*, 11090–11103. [[CrossRef](#)]
35. Lin, C.; Mu, H.; Xiong, R.; Shen, W. A novel multi-model probability battery state of charge estimation approach for electric vehicles using H-infinity algorithm. *Appl. Energy* **2016**, *166*, 76–83. [[CrossRef](#)]
36. Wu, G.; Lu, R.; Zhu, C.; Chan, C. An improved Ampere-hour method for battery state of charge estimation based on temperature, coulomb efficiency model and capacity loss model. In Proceedings of the 2010 IEEE Vehicle Power and Propulsion Conference, Lille, France, 1–3 September 2010; pp. 1–4.

37. Xiong, R.; Sun, F.; Chen, Z.; He, H. A data-driven multi-scale extended Kalman filtering based parameter and state estimation approach of lithium-ion polymer battery in electric vehicles. *Appl. Energy* **2014**, *113*, 463–476. [[CrossRef](#)]
38. Telmoudi, A.J.; Soltani, M.; Ben Belgacem, Y.; Chaari, A. Modeling and state of health estimation of nickel–metal hydride battery using an EPSO-based fuzzy c-regression model. *Soft Comput.* **2019**, *24*, 7265–7279. [[CrossRef](#)]
39. Sun, F.; Xiong, R.; He, H. Estimation of state-of-charge and state-of-power capability of lithium-ion battery considering varying health conditions. *J. Power Sources* **2014**, *259*, 166–176. [[CrossRef](#)]
40. Zhang, Y.Z.; Xiong, R.; He, H.W.; Pecht, M. Validation and verification of a hybrid method for remaining useful life prediction of lithium-ion batteries. *J. Clean. Prod.* **2019**, *212*, 240–249. [[CrossRef](#)]
41. Mohammed, N.; Saif, A.M. Programmable logic controller based lithium-ion battery management system for accurate state of charge estimation. *Comput. Electr. Eng.* **2021**, *93*, 107306. [[CrossRef](#)]
42. Feng, F.; Lu, R.; Zhu, C. A Combined State of Charge Estimation Method for Lithium-Ion Batteries Used in a Wide Ambient Temperature Range. *Energies* **2014**, *7*, 3004–3032. [[CrossRef](#)]
43. Zhang, S.; Guo, X.; Dou, X.; Zhang, X. A data-driven coulomb counting method for state of charge calibration and estimation of lithium-ion battery. *Sustain. Energy Technol. Assessments* **2020**, *40*, 100752. [[CrossRef](#)]
44. Gismero, A.; Schaltz, E.; Stroe, D.-I. Recursive State of Charge and State of Health Estimation Method for Lithium-Ion Batteries Based on Coulomb Counting and Open Circuit Voltage. *Energies* **2020**, *13*, 1811. [[CrossRef](#)]
45. Hinz, H. Comparison of Lithium-Ion Battery Models for Simulating Storage Systems in Distributed Power Generation. *Inventions* **2019**, *4*, 41. [[CrossRef](#)]
46. Tremblay, O.; Dessaint, L.-A.; Dekkiche, A.-I. A Generic Battery Model for the Dynamic Simulation of Hybrid Electric Vehicles. In Proceedings of the IEEE Vehicle Power and Propulsion Conference, Arlington, TX, USA, 9–12 September 2007; pp. 284–289.
47. Zine, B.; Marouani, K.; Becherif, M.; Yahmedi, S. Estimation of Battery Soc for Hybrid Electric Vehicle using Coulomb Counting Method. *Int. J. Emerg. Electr. Power Syst.* **2018**, *19*. [[CrossRef](#)]
48. Baroody, R. *UNLV Theses, Dissertations, Professional Papers, and Capstones*; UNLV: Las Vegas, NV, USA, 2009.
49. Ren, G.; Wang, H.; Chen, C.; Wang, J. An energy conservation and environmental improvement solution-ultra-capacitor/battery hybrid power source for vehicular applications. *Sustain. Energy Technol. Assess.* **2021**, *44*, 100998. [[CrossRef](#)]
50. Coleman, M.; Lee, C.K.; Zhu, C.; Hurley, W.G. State-of-charge determination from EMF voltage estimation: Using impedance, terminal voltage, and current for lead-acid and lithium-ion batteries. *IEEE Trans. Ind. Electron.* **2007**, *54*, 2550–2557. [[CrossRef](#)]